

**MINISTRY OF EDUCATION
AND TRAINING**

**VIETNAM ACADEMY OF
SCIENCE AND TECHNOLOGY**

GRADUATE UNIVERSITY SCIENCE AND TECHNOLOGY



Le Van Dung

**Research synthesis and catalytic characteristics based on
nano titanium dioxide and zirconium metal-organic
frameworks (Zr-MOFs) for application in the treatment of
organophosphorus nerve agents**

SUMMARY OF DISSERTATION ON SCIENCES OF MATTER

Major: Theoretical chemistry and physical chemistry

Code: 9 44 01 19

Hà Nội - 2025

The thesis was completed at: Graduate University Science and Technology - Vietnam Academy of Science and Technology

Supervisors:

1. Supervisor 1: Assoc. Prof. Dr. Dang Tuyet Phuong - Institute of Chemistry, Vietnam Academy of Science And Technology
2. Supervisor 2: Dr. Nguyen Duy Trinh - Nguyen Tat Thanh University

Referee 1: Assoc. Prof. Dr. Le Minh Cam

Referee 2: Assoc. Prof. Dr. Dao Quoc Tuy

Referee 3: Assoc. Prof. Dr. Dao Ngoc Nhiem

The dissertation is examined by Examination Board of Graduate University of Science and Technology, Vietnam Academy of Science and Technology at 9h00 April 22th 2025

The dissertation can be found at:

1. Graduate University of Science and Technology Library
2. National Library of Vietnam

LIST OF THE PUBLICATIONS RELATED TO THE DISSERTATION

1. **Dung Van Le**, Trinh Duy Nguyen, Phuong T. Dang, Pham Thi Hai Yen and Manh B. Nguyen, “Enhancing the Degradation Efficiency of Dimethyl Nitrophenyl Phosphate, a Chemical Warfare Agent Simulant, through Acid Sites in Bimetallic Metal–Organic Framework Ti-MOF-808(Zr): Synergistic Roles of Lewis and Brønsted Acids”, *Applied Surface Science*, **2024**, 655, 159588.
2. **Dung Van Le**, Manh B. Nguyen, Phuong T. Dang, Taeyoon Lee and Trinh Duy Nguyen, “Synthesis of a UiO-66/g-C₃N₄ composite using terephthalic acid obtained from waste plastic for the photocatalytic degradation of the chemical warfare agent simulant, methyl paraoxon”. *RSC Adv*, **2022**, 12, 22367–22376.
3. **Lê Văn Dũng**, Đặng Tuyết Phương, Nguyễn Duy Trinh, Nguyễn Bá Mạnh, “Tổng hợp vật liệu nano TiO₂ và ZrO₂ để phân hủy chất mô phỏng tác nhân thần kinh”, *Tạp chí xúc tác và hấp phụ Việt Nam*, **2022**, 11 (1), 104-109.
4. Bùi Trung Thành, Đặng Thanh Bình, **Lê Văn Dũng**, Nguyễn Xuân Toàn, Lại Văn Cương, Nguyễn Bá Mạnh, “Tổng hợp vật liệu nano TiO₂ ứng dụng để phân hủy chất mô phỏng chất độc thần kinh DMNP”, *Tạp chí Nghiên cứu Khoa học và Công nghệ quân sự (JMST)*, **12/2022**, 84, 42-49.

INTRODUCTION

1. The Urgency of the Thesis

Organic phosphorus compounds (phosphorus organic compounds, organophosphates, OPs) are derivatives of phosphorus (V) and phosphorus (III) used to synthesize a wide range of commercially valuable organic substances like pesticides, insecticides, herbicides, fungicides, flame retardants, surfactants, and pharmaceuticals. In addition, organic phosphorus compounds are also used to produce organophosphorus nerve agents (OPNAs), which are among the highly toxic chemical warfare agents (Chemical Warfare Agents, CWAs).

There have been numerous research studies published on treating OPNAs, which include some basic methods such as adsorption, chemical methods like advanced oxidation, photodegradation, and photo-Fenton, and biological methods. In recent years, scientists have devoted a significant amount of time and effort to developing catalysts capable of effectively decomposing OPNAs. Some studies show that metal oxide nanomaterials or composites containing metal oxide nanomaterials with a large specific surface area can effectively deal with CWAs. Among these, TiO_2 is one of the most versatile and multifunctional oxides, proposed as a promising material with rapid adsorption and effective treatment of CWAs. Recently, Metal-Organic Frameworks (MOFs) have emerged as a potential catalyst for quickly decomposing CWAs due to their superior advantages, including a rich porous structure, high surface area, and the presence of multifunctional ligands. Among these, zirconium-based metal-organic frameworks (Zr-MOFs) and their derivatives, known for their stability and outstanding activity, have received considerable attention for this application. Within the Zr-MOF category, MOF-808(Zr) stands out significantly, with network nodes formed by Zr ions, which can combine with various other metal ions. The synergy of two metal ions at the same network node enhances its activity. Thus, MOF-808(Zr) modified with different metal ions offers outstanding benefits like a large specific surface area, chemical stability, and high porosity, making it a particularly effective material for environmental

treatment in general and decomposition of organophosphorus compounds in particular. In this dissertation, nano TiO₂, Zr-MOFs catalysts, and some of their modified forms are synthesized and applied as catalysts in decomposing simulants of OPNAs (Dimethyl p-nitrophenyl phosphate, DMNP).

2. The objective of the thesis

The synthesis of catalyst materials based on titanium oxide, Zr-MOFs, and some modified forms of them has been developed, aimed at being used as catalysts in the degradation of simulants for nerve agents like Dimethyl p-nitrophenyl phosphate (DMNP) in military applications, paving the way for potential real applications in degrading organophosphorus compounds in both industrial and civil sectors.

3. Main research content of the thesis

(1) Synthesis of TiO₂ nanoparticles, Zr-MOFs from a self-synthesized linker (Zr-MOFs-TH) including UiO-66C and UiO-66C/g-C₃N₄, and Zr-MOFs from commercial linkers (Zr-MOFs-TM) including UiO-66, UiO-66-NH₂, UiO-67, Zr-NDC, NU-1000, MOF-808(Zr), and Ti-MOF-808(Zr) aimed at decomposing DMNP.

(2) The structural characteristics and crystal morphology of the synthesized materials were analyzed using modern physicochemical methods.

(3) The catalytic activity of the synthesized materials was determined by their ability to decompose DMNP.

(4) The stability of the catalytic materials during the DMNP decomposition process was evaluated.

(5) A reaction mechanism for the decomposition of DMNP on the synthesized catalyst was proposed.

CHAPTER 1. OVERVIEW

The overview section gathers and analyzes studies both domestically and internationally related to the issues addressed in the thesis.

1.1. Nerve agents and organophosphorus nerve agent simulants

1.2. Methods for decomposing organophosphorus nerve agents

1.3. Titanium oxide nanomaterials for decomposing organophosphorus nerve agents

1.4. Metal - organic framework materials applied for decomposing organophosphorus nerve agents

1.5. Current state of research in the country

CHAPTER 2. EXPERIMENT AND RESEARCH METHODS

2.1. Experiment

2.2. Equipment and tools

2.3. Material Synthesis Method

In this section, the thesis presents the method for synthesizing TiO_2 nanoparticles, the Zr-MOFs synthesized from self-synthesized linker (Zr-MOFs-TH) including UiO-66C, UiO-66C/g- C_3N_4 , and from commercial linkers (Zr-MOFs-TM) including UiO-66, UiO-66- NH_2 , UiO-67, Zr-NDC, NU-1000, MOF-808(Zr), and Ti-MOF-808(Zr).

2.3.1. Nano titanium oxide (TiO_2)

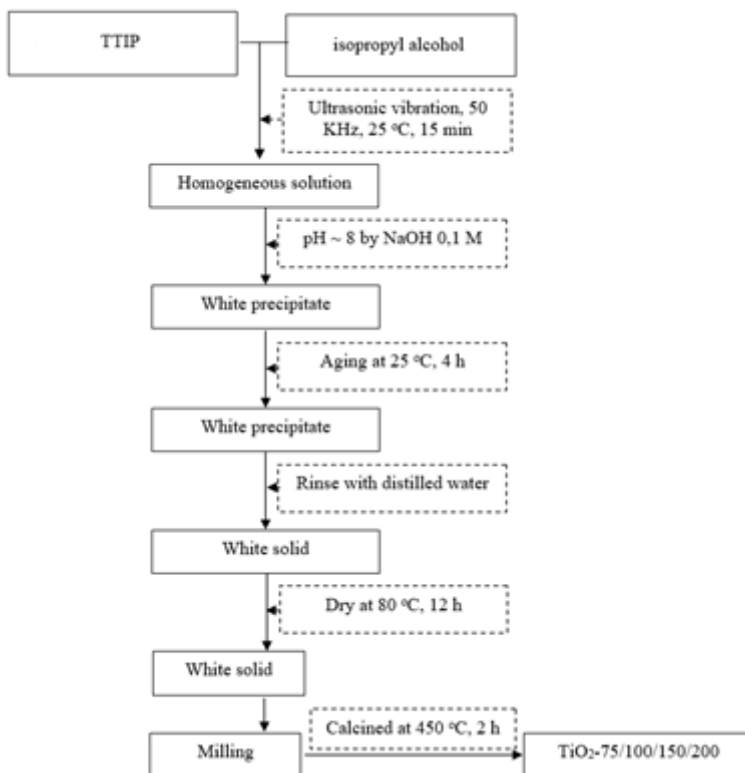


Figure 2.1. Synthesis diagram of TiO_2

2.3.2. Zr-MOFs-TH

2.3.2.1. Synthesis of H_2BDC from polyethylene terephthalate (PET) water bottles

The H_2BDC linker is synthesized from water bottles (PET plastic), and this linker is used to synthesize UiO-66C and UiO-66C/g- C_3N_4 .

2.3.2.2. Preparation of g- C_3N_4

g- C_3N_4 is prepared from urea and NH_4Cl , and the product is used to synthesize UiO-66C/g- C_3N_4 .

2.3.2.3. Synthesis of UiO-66C and UiO-66C/g- C_3N_4

UiO-66C is synthesized according to the diagram in Figure 2.5.

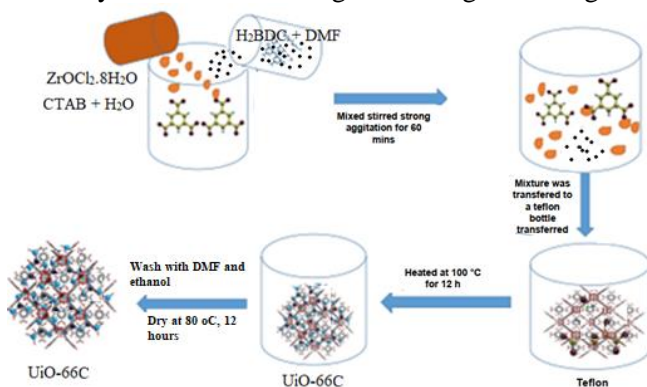


Figure 2.5. Synthesis diagram of UiO-66C/g- C_3N_4

UiO-66C/g- C_3N_4 was synthesized according to the schematic in Figure 2.6

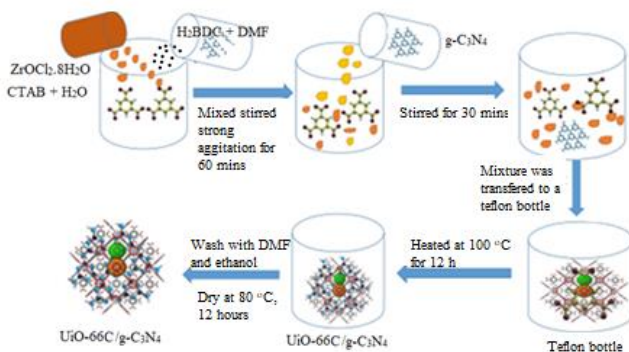


Figure 2.6. Synthesis diagram of UiO-66C/g- C_3N_4

2.3.3. Zr–MOFs-TM

Zr–MOFs synthesized from commercial linkers include UiO-66, UiO-66-NH₂, UiO-67, Zr–NDC, NU-1000, and MOF-808(Zr) as shown in the schematic in Figure 2.7. Ti–MOF-808(Zr) is synthesized according to the schematic in Figure 2.8.

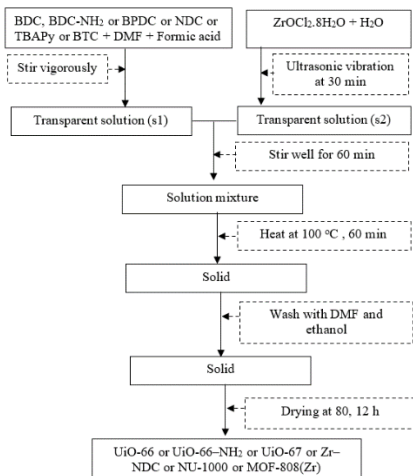


Figure 2.7. Synthesis diagram of UiO-66 or UiO-66-NH₂ or UiO-67 or Zr–NDC or NU-1000 or MOF-808(Zr)

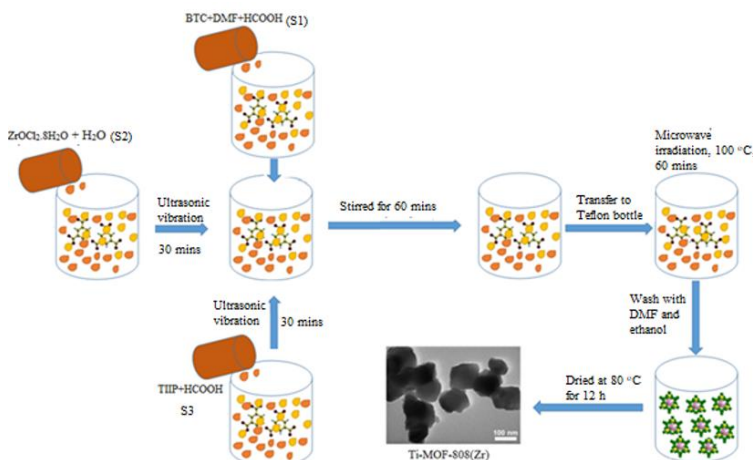


Figure 2.7. Synthesis diagram of Ti-MOF-808(Zr)

Table 2.4. Amount of precursor, molar ratio Ti/Zr (%) in the synthesis of Ti–MOF-808(Zr)

H ₃ BTC (g)	ZrOCl ₂ .8H ₂ O (g)	TTIP (g)	Mole ratio Ti/Zr (%)	Sample symbol
1.68	7.573	0.134	2	2% Ti–MOF-808(Zr)
1.68	7.418	0.262	4	4% Ti–MOF-808(Zr)
1.68	7.109	0.505	8	8% Ti–MOF-808(Zr)

2.4. Characterization methods

2.4.1. X-ray diffraction (XRD)

The XRD method is used to determine the crystal structure of materials (lattice parameters, crystal size, lattice type) and to analyze the qualitative and quantitative phase composition present in the synthesized material samples. The synthesized materials in this thesis were measured using a Bruker D8 Advance device with Cu K α radiation, $k=1.5406$ Å, over an angular range of $2\theta \sim 5 \div 50^\circ$ at the University of Science - Vietnam National University.

2.4.2. Fourier Transform Infrared Spectroscopy (FT-IR)

FT-IR is used to study the presence of functional groups and possible bonds in catalyst samples. The synthetic material samples in this thesis were measured using an FT-IR spectrometer 4700/JASCO, with a resolution of 1 cm^{-1} , over a wavelength range of 400 to 4000 cm^{-1} , at the Institute of Chemistry-Vietnam Academy of Science and Technology.

2.4.3. Scanning Electron Microscopy (SEM) and Transmission Electron Microscopy (TEM)

Determining the crystal morphology of material samples. In this study, SEM images were taken using the TOPCON ABT-150 Scanning Electron Microscope, and TEM images were captured on the TEM 1010 (Japan), with a magnification of 80,000 times, at the Central Institute of Hygiene and Epidemiology.

2.4.4. Adsorption - Desorption Isotherms of Nitrogen

Surface parameters such as specific surface area, volume, pore size distribution, and the porous nature of the material in the thesis were

determined using nitrogen adsorption and desorption isotherms at a temperature of 77 °K, on a Tristar-3030 (Micromeritics-USA) measurement device at the Institute of Chemistry-Vietnam Academy of Science and Technology.

2.4.5. X-ray Photoelectron Spectroscopy (XPS)

XPS is used to determine information about the basic composition, chemical state, and electronic state of elements on the surface of materials, by recording the binding energy of electrons emitted from the surface of the sample after being exposed to X-ray radiation. The samples were measured using XPS on a Thermo VG Multilab 2000 device in the UK.

2.4.6. Diffuse Reflectance Spectroscopy for Ultraviolet-Visible Light (UV-Visible Diffuse Reflectance Spectroscopy, UV-Vis DRS)

The optical properties and the band gap energy (E_g) of the material are determined using UV-Vis DRS spectra. UV-Vis DRS measurements are carried out using a UV-2600 instrument (Shimadzu, Japan), within the wavelength range of 200 to 800 nm, at the Institute of Physics-Vietnam Academy of Science and Technology.

2.4.7. Photoluminescence Spectroscopy (Photoluminescence, PL)

PL spectra are used to determine the recombination of e^-/h^+ pairs. In this study, PL measurements are taken using a Cary Eclipse fluorescence spectrophotometer (Varian), with an excitation wavelength of 320 nm, and data are recorded in the range of 350 to 600 nm, at the Institute of Chemistry-Vietnam Academy of Science and Technology.

2.4.8. Energy Dispersive X-ray Spectrometry (EDS)

The elemental composition and the weight percentage of elements in the material samples are determined using EDS. In this thesis, EDS is measured at an accelerating voltage of 15 keV, with a resolution from 10 to 100 μ m on a Hitachi S-4800 scanning electron microscope, at the Institute of Materials Science-Vietnam Academy of Science and Technology.

2.4.9. Thermogravimetric and differential thermal analysis (TGA-DTA)

It is permissible to use differential thermal analysis (DTA) and

thermogravimetric analysis (TGA) to determine the durability of materials. The material samples in the thesis were analyzed on the LINSEIS STA PT1600 thermal analyzer at the Faculty of Chemical Technology-Hanoi University of Industry. This analysis was conducted at a temperature range from room temperature to 800 °C in an air environment and at a heating rate of 10 °C/min.

2.4.10. Temperature programmed NH₃ desorption method (TPD-NH₃) and FTIR analysis of acetonitrile-d₃(CD₃CN) adsorption

TPD-NH₃ is used to consider the acid force and acidity on the catalyst. CD₃CN analysis to determine the number of Brønsted and Lewis acid centers on the catalyst surface. In this thesis, the NH₃ desorption method was performed on Autochem 2020 equipment (Micromeritics-USA), analyzing CD₃-CN adsorption on the Nicolet Nexus 670 Fourier transform infrared spectrometer (FT-IR) at the Institute of Chemistry, Vietnam Academy of Science and Technology.

2.5. Determination of the E_{CB} and E_{VB} of the g-C₃N₄, UiO-66C, and UiO-66C/g- C₃N₄-30%

In the study of thesis, to determine the conduction band potential (E_{CB}) of g-C₃N₄, UiO-66C, and UiO-66C/g- C₃N₄-30% was performed as follows:

Preparation of electrodes used for Mott-Schottky measurement: disperse 1 mg of the material to be measured in 1 mL of ethanol, apply to FTO membrane and let it dry naturally. Then, the FTO membrane is placed in 0.1 M Na₂SO₄ solution and Mott-Schottky is measured in the potential range from -1.5 to +1.5 V (vs NHE), frequency 500 Hz, on Autolab equipment at the Institute of Chemistry, Vietnam Academy of Science and Technology. From the Mott-Schottky diagram determined from the potential measurement, the conduction band potential (E_{CB}) of g-C₃N₄, UiO-66C, and UiO-66C/g- C₃N₄-30% are determined, and the valence band potential (E_{VB}) is determined according to formula (2.7).

2.6. LC-MS determined products formed during DMNP degradation

DMNP hydrolysis and catalytic degradation products were determined by liquid chromatography-mass spectrometry (LC-MS). In this thesis, LC-MS results were analyzed with a Thermo-Fisher system (XEVO TQ-XS LC-MS). The mobile phase was water with a flow rate of 0.1 mL min⁻¹ at the

Central Drug Testing Institute.

2.7. Determine the catalytic activity of the material

2.7.1. Nano titanium oxide (TiO_2) material

Add 30 mg of TiO_2 (75 or 100 or 150 or 200) into 1 mL of water (pH = 7, temperature 25 °C) and stir at 1300 rpm with a magnetic stirrer for 15 minutes. Add 6.2 mg of DMNP and irradiate with a power of 30 W using a fluorescent lamp; the intensity of the incident light is about 2880 Lux, and the simulated sunlight is irradiated throughout the reaction. The distance from the light source to the solution surface is about 15 cm. Next, take 20 μL of the reaction mixture and dilute with 10 mL of 0.15 M NEM to determine the concentration of 4-nitrophenol. NEM survey values 0 M, 0.15 M, 0.3 M, 0.45 M, and 0.6 M were obtained by adding 0 μL , 17 μL , 34 μL , 50 μL and 68 μL NEM (99 %) into 30 mg of TiO_2 -100 catalyst and 1 mL of water (pH = 7, temperature 25 °C). The order of execution is similar to the activity determination of TiO_2 samples. The reuse durability of the material is determined by after each activity determination, TiO_2 -100 is cleaned with NEM 1M and ethanol, then dried at 80 °C, 12 hours to use for the reaction cycle next.

2.7.2. Zr-MOFs-TH

2.5 mg each of UiO-66C and UiO-66C/g- C_3N_4 (10, 20, 30, 40%) and 1 mL of water (pH = 7) were added to a 2 mL reactor and stirred at 1300 rpm using a machine. Stir magnetically for 15 minutes. Add 6.2 mg of DMNP and irradiate with a power of 30 W using a fluorescent lamp; the incident light intensity is about 2880 Lux, and simulated sunlight is irradiated throughout the reaction. The distance from the light source to the surface of the reaction solution is about 15 cm. Then take 20 μL of the reaction mixture and dilute with 10 mL of 0.15 M NEM to determine the 4-nitrophenol concentration. Evaluate the influence of catalyst content: Samples of 0.84 mg, 1.68 mg, 2.5 mg, 3.36 mg, 4.2 mg, and 5.04 mg UiO-66C/g- C_3N_4 -30% were investigated for metabolism 6, 2 mg is present in 1 mL of solution. Determining the reuse durability of the catalyst: Use the catalyst content with the best conversion efficiency to determine the reuse durability. UiO-

66C/gC₃N₄-30% after decomposition DMNP was washed many times with NEM solution, ethanol, and dried at 80 °C for 12 hours for the next cycle.

2.7.3. Zr-MOFs-TM

Add 2.04 mg of UiO-66 (or UiO-66-NH₂, UiO-67, Zr-NDC, NU-1000, MOF-808(Zr), and (2%, 4 % and 8%)Ti-MOF- 808(Zr)) into 1 mL of water and stir at 1300 rpm with a magnetic stirrer for 15 minutes. Add 6.2 mg and 4 μ L NEM (99%). After 10 seconds of reaction, remove 20 μ L of the reaction mixture and dilute with 10 mL of 0.15 M NEM to determine the 4-nitrophenol concentration. Samples of 0.68 mg, 1.36 mg, 2.04 mg, 2.72 mg, 3.4 mg, and 4.08 mg of 4%Ti-MOF-808(Zr) catalyst were used for the investigation. to evaluate the influence of catalyst content. Investigate the effect of NEM buffer concentration (0.00, 0.15, 0.30, 0.45, 0.60, and 0.80 M). The pH of the solution was also investigated from 3 to 10. In addition, the reuse durability of the 4%Ti-MOF-808(Zr) sample was investigated.

2.8. Determine the role of free radicals in the ability to decompose DMNP

The role of free radicals in the DMNP decomposition reaction with UiO-66C/gC₃N₄-30% was determined by electron trap experiments. The "electron trap" experiment is performed similarly to section 2.6.2 Zr-MOFs-TH. However, to determine the role of reactive radicals, before the reaction, an amount of toxic radical scavenger is added, and the reaction is similar to section 2.6.2. Specifically, trapping agents including ammonium oxalate monohydrate (AO), tert-butanol (TBA), potassium dichromate (K₂Cr₂O₇), and 1,4-benzoquinone (BQ), with a concentration of 1 mM, are used to capture h⁺, •OH, e⁻, and •O²⁻, respectively. The corresponding electron capture substances will affect the DMNP conversion efficiency. From this result, the role of each free radical in the decomposition process will be evaluated.

CHAPTER 3. RESULTS AND DISCUSSION

3.1. Titanium oxide nanomaterial (TiO₂)

3.3.1. Characteristics of crystal structure and morphology

The TiO₂ nano X-ray diffraction pattern shows diffraction peaks at 2 θ angle, the characteristic reflection plane of the anatase phase of TiO₂. The N₂

adsorption-desorption isotherms of TiO_2 material have the form of type IV hysteresis lines, IUPAC classification. N_2 adsorption-desorption isotherms at partial pressures $P/P_0 \sim 0.4$ to 1 exhibit a hysteresis loop commonly found in mesoporous materials. In particular, the TiO_2 -100 sample has a specific surface area, capillary volume, and largest capillary diameter of $139 \text{ m}^2/\text{g}$, $0.247 \text{ cm}^3/\text{g}$, and 7.12 nm , respectively. SEM analysis results show that TiO_2 has a particle size of $20 \div 30 \text{ nm}$, a spherical shape, and a quite uniform size. Meanwhile, the UV-Vis DRS analysis results obtained the optical band gap of nanomaterial samples TiO_2 -200, TiO_2 -150, TiO_2 -100, and TiO_2 -75 respectively, 3.20, 3.15, 3.05, and 3.06 eV. The band gap of TiO_2 decreases as the TTIP concentration decreases, which can be explained by the decrease in the crystal grain size of TiO_2 material.

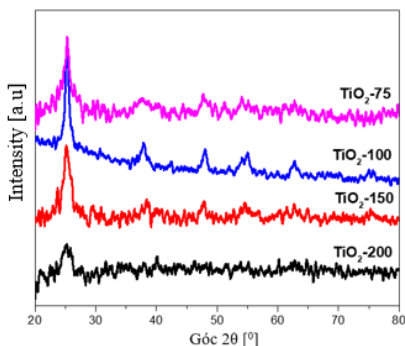


Figure 3.1. XRD patterns of TiO_2 nanomaterial samples

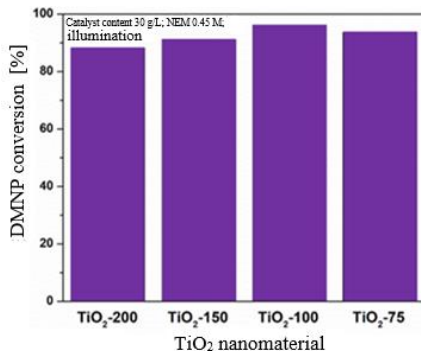


Figure 3.8. DMNP conversion rate of nano TiO_2

3.1.2. Catalytic activity of TiO_2 nanomaterial

Determining the catalytic activity (Figure 3.8) shows that TiO_2 nanomaterial has a relatively high ability to convert DMNP, reaching over 88% after 120 minutes of reaction. Specifically, the conversion on the TiO_2 -(200, 150, 100 and 75) catalyst reached 88.22, 91.23, 96.14 and 93.63%, respectively. Among them, the TiO_2 -100 catalyst achieved the highest efficiency (96.14%). This can be explained because this material has surface parameters (specific surface area, pore size) that are the largest, thus facilitating the diffusion of DMNP onto the catalyst. Determining factors

affecting conversion ability shows that TiO_2 -100 has the highest conversion efficiency (96.14%) under 0.45 M NEM solution, 120 minutes of illumination. This catalyst has the durability to be reused for up to 4 cycles (conversion still reaches over 90%).

3.2. Zr-MOFs-TH materials

3.2.1. Characteristics of the structure and crystal morphology of materials $g\text{-C}_3\text{N}_4$, UiO-66C and UiO-66C/ $g\text{-C}_3\text{N}_4$

The results of X-ray analysis show that the characteristic peak of the $g\text{-C}_3\text{N}_4$ phase was detected, proving that the UiO-66C/ $g\text{-C}_3\text{N}_4$ material was successfully synthesized. Furthermore, it was observed that the peak intensity at 27.3° increased as the $g\text{-C}_3\text{N}_4$ content in the material increased from 10 to 40 wt%. These results indicate that the UiO-66C crystal structure changes insignificantly when $g\text{-C}_3\text{N}_4$ is added. The FT-IR spectrum also shows that changing the $g\text{-C}_3\text{N}_4$ content in the range from 10 to 40% by weight does not significantly affect the original structure of UiO-66C. SEM and TEM images show that UiO-66C has a diameter of 80 to 120 nm, while $g\text{-C}_3\text{N}_4$ sheets have uneven lengths. For UiO-66C/ $g\text{-C}_3\text{N}_4$ (10, 20, 30, 40%) samples, there are dark areas on the micrograph of UiO-66C crystals mounted onto $g\text{-C}_3\text{N}_4$ plates, and brighter edges correspond to $g\text{-C}_3\text{N}_4$ plates.

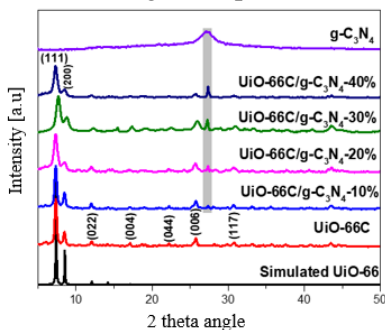


Figure 3.12. XRD diagram of material samples UiO-66C and UiO-66C/ $g\text{-C}_3\text{N}_4$

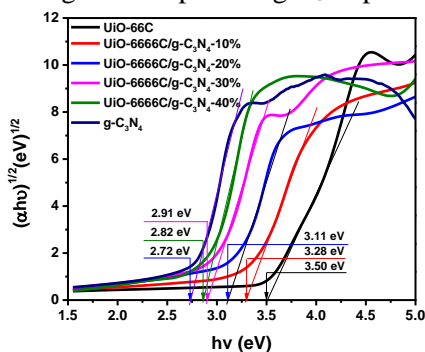


Figure 3.20. Eg calculation chart of UiO-66C and UiO-66C/ $g\text{-C}_3\text{N}_4$

Meanwhile, UiO-66C/g-C₃N₄-40% shows that there is a concentration of UiO-66C nanoparticles into large particles of 100 to 150 nm. The results of adsorption-desorption isotherm analysis show that UiO-66C has the highest specific surface area (S_{BET}) of 1440 m²/g, pore volume (V_{pore}) of 1.05 cm³/g and wide The smallest average capillary according to the BJH model (D_{pore}) is 3.44 nm. Sample UiO-66C/g-C₃N₄(10, 20, 30, 40%) has S_{BET} ranging from 583 to 1162 m²/g, V_{pore} from 0.79 to 1.49 cm³/g and D_{pore} from 4.08 ÷ 5.56 nm. Therefore, the attachment of UiO-66C onto g-C₃N₄ sheets (UiO-66C/g-C₃N₄(10, 20, 30, 40%) significantly reduces S_{BET} compared to unmodified UiO-66C. However, V_{pore} increased from 1.05 to 1.49 cm³/g, and D_{pore} increased from 3.44 to 4.08 nm.

XPS analysis results also showed that the characteristic bonds Zr–O, C–N=C or C₂–NH appeared, indicating that UiO-66C was successfully attached to g-C₃N₄. The results also show that there is a change of electrons from g-C₃N₄ to UiO-66C. From UV-Vis DRS, E_g of g- C₃N₄ and UiO-66C are 2.72 and 3.50 eV, respectively, and UiO-66C/g- C₃N₄ (10, 20, 30, 40 %) is 2.82 ÷ 3.28 eV. The results show that the E_g of UiO-66C/g- C₃N₄ (10, 20, 30, 40 %) are located in the E_g region of UiO-66C and g- C₃N₄, indicating successful hybridization of UiO-66C and g- C₃N₄. The E_g of UiO-66C/g- C₃N₄ sample is lower than that of unmodified UiO-66C. Furthermore, the E_g of UiO-66C/g- C₃N₄ (10, 20, 30, 40 %) decreased as the g- C₃N₄ content increased. This shows that when attaching UiO-66C to g- C₃N₄, the material has better optical properties (due to reducing E_g). Besides, the PL photoluminescence spectrum results also showed that the emission intensity at wavelength 440 nm decreased significantly after attaching UiO-66C to g- C₃N₄; the recombination of the e⁻/h⁺ pair in the material is reduced due to the electron capture of g-C₃N₄ by UiO-66C. In addition, sample investigation by EDS and EDS mapping showed that the synthesized samples were pure and the elements were evenly distributed in the material.

3.2.2. Catalytic activity of g-C₃N₄, UiO-66C, UiO-66C/g-C₃N₄

The survey of catalytic activity (Figure 3.25) showed that DMNP conversion efficiency reached 28.20% and 54.65% for g-C₃N₄ and UiO-66C

after 60 min of illumination. The half-life of DMNP on UiO-66C is about 40 min, while UiO-66C/g- C_3N_4 (10, 20, 30, 40%) samples increased from 86.84% to 98.55%, in which Sample UiO-66C/g- C_3N_4 -30% achieved the highest efficiency. The increased performance for the samples attached to g- C_3N_4 was attributed to their increased absorption of visible light. Furthermore, the capillary size of these samples is improved, which facilitates phase contact of the reactants instead of contact between the catalyst and the phosphate ester bond in the organophosphorus compound, which only takes place on the outer surface of the catalyst. In addition, UiO-66C/g- C_3N_4 samples contain octahedral oxo- Zr_6 clusters, which are Lewis acids, which cleave the phosphate ester bond in DMNP.

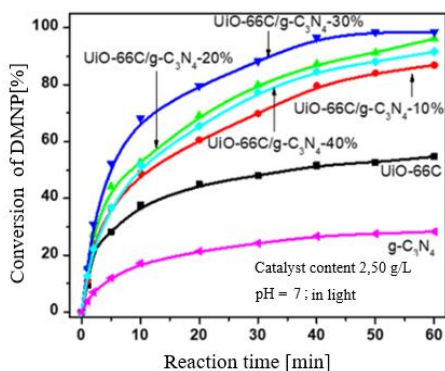


Figure 3.25. Conversion of DMNP by g- C_3N_4 , UiO-66C and UiO-66C/g- C_3N_4 (10, 20, 30, 40%)

A survey of influencing factors shows that catalyst content and, lighting/no lighting have a significant impact on the conversion efficiency of the material. The results show that the heterogeneous catalyst UiO-66C/g- C_3N_4 -30% gives the best DMNP conversion efficiency (98.9%, $t_{1/2} = 2.17$ min) with the optimal condition being the amount of catalyst 4.20 g/L, visible light irradiation. This catalyst has relatively good reuse durability; after 5 reaction cycles, the efficiency still reaches over 98%.

Proposed mechanism (detailed in the synthesis report); however, the photocatalytic principle of UiO-66C/g- C_3N_4 -30% as well as other

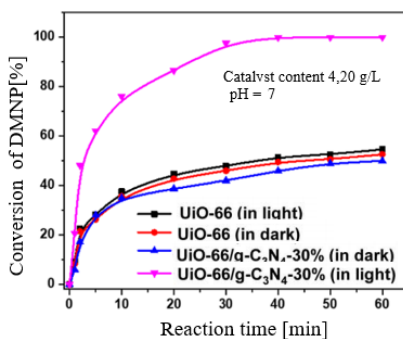


Figure 3.28. Dependence on light irradiation of DMNP conversion efficiency using UiO-66C and UiO-66C/g- C_3N_4 -30% materials

photocatalytic materials, i.e., will create e^-/h^+ pairs that act as reducing agents and oxidizing agents. In the photocatalytic mechanism of the UiO-66C/g-C₃N₄-30% heterogeneous catalytic material, attaching UiO-66C to g-C₃N₄ limited the recombination of the e^-/h^+ pair in UiO-66C (part of the e^- in the CB of UiO-66C combines with h^+ in the VB of g-C₃N₄), thereby contributing to enhancing the activity of the material.

3.3. Zr-MOFs-TM materials

In this section, the structural characteristics, crystal morphology, and catalytic activity of Zr-MOFs-TM including, UiO-66, UiO-66-NH₂, UiO-67, Zr-NDC, NU-1000, and MOF-808(Zr) are presented.

3.3.1. Characteristics of crystal structure and morphology

Typical results include X-ray diffraction, TEM images, N₂ adsorption-desorption isotherm, and X-ray scattering spectrum showing UiO-66, UiO-66-NH₂, UiO-67, MOF-808(Zr), and Zr-NDC were successfully synthesized. Among them, MOF-808(Zr) has the largest specific surface area and pore volume of 1756 m²/g and 1.159 cm³/g, respectively, and has the highest number of Zr centers (% wt accounts for 36.19 % in these Zr-MOFs).

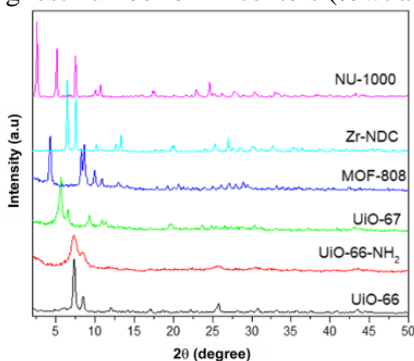


Figure 3.35. XRD diagram

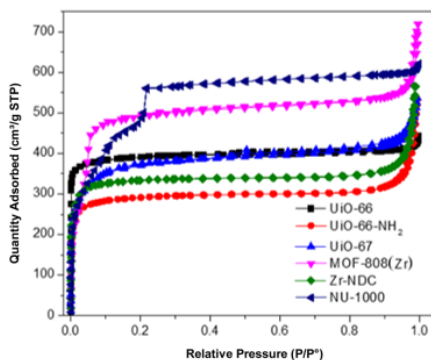


Figure 3.37. N₂ adsorption-desorption isotherm

3.3.2. Zr-MOFs-TM catalytic activity

The results of determining the activity (Figure 3.41) show that the material MOF-808(Zr) has the fastest half-life (0.47 min) and completely decomposes in 3.00 min. Therefore, MOF-808(Zr) was chosen to be

modified with Ti^{4+} metal ion to create bimetallic MOFs, thereby creating a material with advantages such as having many active centers and stability, chemistry, and high porosity to increase catalytic activity. Therefore, MOF-808(Zr) modified with Ti^{4+} ions (Ti-MOF-808(Zr) synthesized from a commercial linker will be discussed in the next section of the thesis.

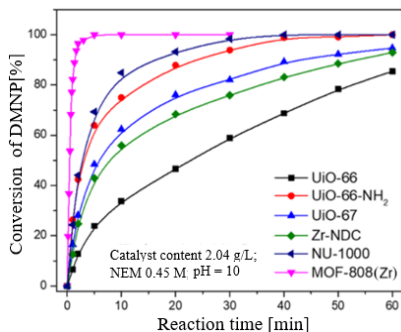


Figure 3.41. DMNP conversion efficiency of catalysts UiO-66, UiO-66-NH₂, UiO-67, Zr-NDC, NU-1000, and MOF-808(Zr)

3.4. Material Ti-MOF-808(Zr)

3.4.1. Characteristics of structure and crystal morphology of material Ti-MOF-808(Zr)

The results of X-ray analysis show that MOF-808 (Zr) is not broken during the denaturation process. Furthermore, the diffraction peaks have a slight shift toward larger 2θ angles. This shift is due to the smaller ionic radius of Ti^{4+} (0.68 Å) compared to Zr^{4+} (0.82 Å), leading to a contraction of the crystal lattice in the MOF-808 (Zr) structure. Results of FT-IR spectroscopy analysis of MOF-808(Zr) and (2, 4, 8%)Ti-MOF-808(Zr) show that both of these material samples have unique characteristics. Meanwhile, for the samples (2%, 4%, and 8%) Ti-MOF-808(Zr), the characteristic vibrations of Zr-O fluctuated in the range of 666 to 662 cm^{-1} showing a shift slightly between samples, which may be due to the presence of Ti in different concentrations in the Zr-MOFs framework. TEM and SEM

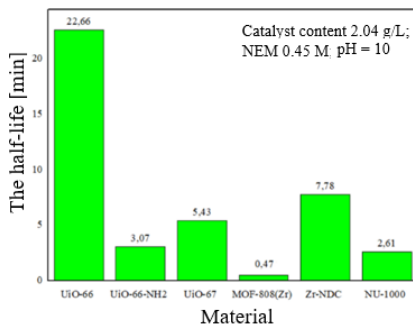


Figure 3.42. The half-life of DMNP on UiO-66, UiO-66-NH₂, UiO-67, MOF-808(Zr), Zr-NDC, and NU-1000 catalysts

results show that these material samples have an average grain size of about 100 nm; moreover, the samples (2, 4, 8%)Ti–MOF-808(Zr) change in morphology insignificantly compared to MOF-808(Zr). The study also showed that the specific surface area (S_{BET}) of MOF-808(Zr) is 1756 m²/g and the pore volume is 1.159 cm³/g. Meanwhile, the materials (2%, 4%, and 8%)Ti–MOF-808(Zr) fluctuate between 1741 ÷ 1406 m²/g and 1.082 ÷ 0.913 cm³/g. It is worth noting that the surface area and pore volume of MOF-808(Zr) containing Ti decreased slightly, which may be due to the smaller ionic radius of Ti⁴⁺ (0.68 Å) compared to Zr⁴⁺ (0.81 Å).

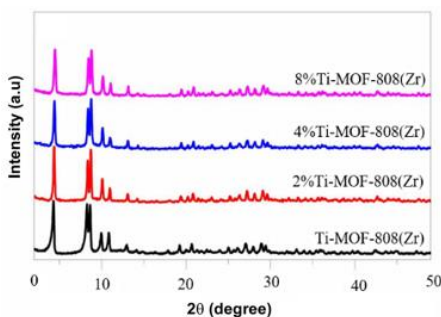


Figure 3.43. XRD patterns of MOF-808(Zr) and (2, 4, 8%)Ti–MOF-808(Zr)

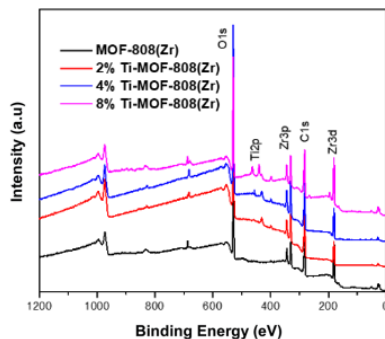


Figure 3.49. XPS spectrum of MOF-808(Zr) and Ti–MOF-808(Zr)

XPS spectrum shows the presence of Ti⁴⁺ ions in Ti–MOF-808(Zr) material samples. Notably, the binding energy of Zr 3d shifts to higher values as the Ti content in the sample increases. This phenomenon is because Ti has a higher electronegativity (1.54) than Zr (1.33), leading to the electron density around the Zr phase being pulled towards the Ti phase. This result shows that the electrons in the material (2, 4, 8%)Ti–MOF-808(Zr) transfer from the Zr phase to the Ti phase. In addition, sample investigation by EDS and EDS mapping showed that the synthesized samples were pure and the elements were evenly distributed in the material.

The results of thermogravimetric and differential thermal analysis show that the materials MOF-808 and 4%Ti–MOF-808(Zr) have thermal stability above 500 °C.

The acid properties of the samples (2, 4, 8%)Ti–MOF-808(Zr) and MOF-808(Zr) were determined by the temperature-programmed NH_3 desorption method (NH_3 -TPD). All samples MOF-808(Zr) and (2, 4, 8%)Ti–MOF-808(Zr) have peaks in the range of 100–160 °C and 180–260 °C. These peaks were assigned to the weak and moderate acidity of the $\mu_3\text{-OH}$, $-\text{OH}_2$, and $-\text{OH}$ groups. Interestingly, the intensity of these peaks increases linearly with increasing Ti content, indicating that the number of weak and medium acid sites is higher. These results indicate that the combination of Zr and Ti improved the number of acid sites on the catalyst surface. The number of Brønsted and Lewis acid centers on the catalyst surface of samples MOF-808(Zr) and (2, 4, 8%)Ti–MOF-808(Zr) was determined by FTIR analysis of adsorption acetonitrile- d_3 (FTIR- CD_3CN). The CD_3CN adsorption intensity at wavelengths 2308 and 2272 cm^{-1} corresponding to the Lewis and Brønsted acid centers of Ti–MOF-808(Zr) samples increased significantly when increasing the Ti content from 0 to 4 % mol. This increase indicates an increase in the amount of Lewis and Brønsted acid centers in the (2, 4, 8%)Ti–MOF-808(Zr) sample. The increase in the number of Lewis and Brønsted acid sites was achieved by incorporating $-\text{OH}$ groups into the metal nodes during hydrothermal synthesis and introducing Ti^{4+} into the MOF-808(Zr) framework. The study also found that, as the total number of acid sites increased, the half-life of DMNP decreased, meaning the decomposition rate increased, in which the 4%Ti–MOF-808(Zr) sample had the lowest half-life (0.305 min). Meanwhile, the Lewis acid center in the catalyst plays a decisive role in decomposing DMNP.

Table 3.14. Acidity of MOF-808(Zr) and Ti–MOF-808(Zr).

Sample	MOF-808(Zr)	2% Ti–MOF-808(Zr)	4% Ti–MOF-808(Zr)	8% Ti–MOF-808(Zr)
TPD-NH ₃ (mmol/g)				
Weak acid	0.421	0.456	0.500	0.506
Medium acid	0.223	0.251	0.266	0.281
Total	0.644	0.707	0.766	0.787

3.4.2. Catalytic activity of Ti–MOF-808(Zr) material

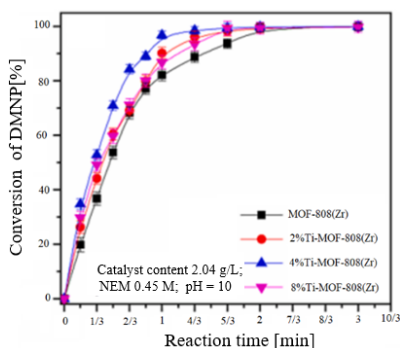


Figure 3.61. DMNP conversion efficiency over reaction time on samples MOF-808(Zr) and (2, 4, 8%)Ti–MOF-808(Zr)

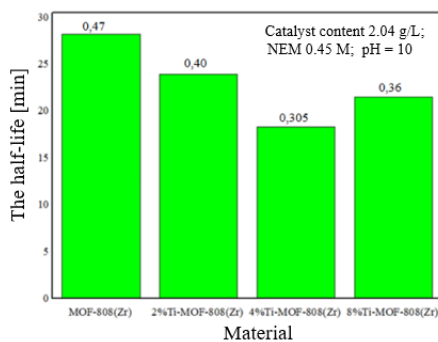


Figure 3.62. DMNP half-life on MOF-808(Zr) and (2, 4, 8%)Ti–MOF-808(Zr) samples

Surveying the catalytic activity (Figure 3.61) shows that the decomposition rate of DMNP with MOF-808(Zr) and (2, 4, 8%)Ti–MOF-808(Zr) occurs very quickly. This rapid degradation may be due to the inherent properties of the MOF-808(Zr) material. These properties include the presence of numerous Zr₆ Lewis acid clusters and hydroxyl (μ_3 -OH) bonds on the Zr₆ nodes, which contribute to accelerating hydrolysis catalysis. Notably, Ti–MOF-808(Zr) samples exhibited significantly faster DMNP degradation rates than MOF-808(Zr), due to their higher Lewis acid center

density. Specifically, the decomposition half-lives of samples MOF-808(Zr), 2%Ti–MOF-808(Zr), 4%Ti–MOF-808(Zr) and 8%Ti–MOF-808(Zr) are 0.47, 0.40, 0.305, and 0.36 minutes, respectively. It can be seen that when the Ti content increases from 0 to 4%, the DMNP decomposition half-time decreases from 0.47 to 0.305 minutes, meaning the decomposition rate increases. This increased decomposition rate may be due to the increased Ti content in MOF-808(Zr), leading to an increase in the number of Lewis and Brønsted acid centers in the material and thus an increased rate of DMNP decomposition. Overall, all MOF-808(Zr) and (2, 4, 8%)Ti–MOF-808(Zr) samples showed superior efficiency in converting DMNP to 4-nitrophenol and dimethyl phosphate within 1.67 minutes.

Determination of influencing factors shows that the optimal conditions when catalyst content (2.72 g/L), NEM solution concentration (0.45 M), and pH = 9, the catalyst is 4% Ti–MOF-808(Zr), showed the best DMNP metabolism efficiency with a half-life of 0.25 minutes, and after 1.34 minutes complete metabolism. This catalyst also provides relatively good reuse durability; after 6 reaction cycles, the efficiency still reaches over 98%.

The mechanism of DMNP decomposition on 4%Ti-MOF-808(Zr) material is proposed (details are presented in the synthesis report); however, the main mechanism is nucleophilic attack on the --O=P , which leads to weakening of RO=P and P^{5+} bonds, and after the addition of water to SBU, the DMNP simulant is hydrolyzed and releases H-X (4-nitrophenol). Finally, the P-OAr chemical bond ($\text{ArO} = 4\text{-nitrophenol}$) is cleaved, and the decomposition products are continuously released from the active site to regenerate the next catalytic reaction. During the reaction, NEM buffer solution can act as a base to neutralize the acidic products produced to accelerate the reaction rate and remove water protons to facilitate the hydrolysis process.

From previously published results and data obtained in the thesis, a comparison of DMNP conversion efficiency is given in Table 3.16. The data presented in Table 3.16, it can be seen that the conversion efficiency of 4%Ti–MOF-808(Zr) is significantly higher than previously published

materials, emphasizing the special efficiency of the material. This acts as a catalyst to quickly remove DMNP. Thus, 4%Ti–MOF-808(Zr) has the potential to be used as a material to treat organophosphorus nerve agents quickly and effectively. Meanwhile, photocatalytic decomposition of DMNP on UiO-66C/g- C_3N_4 material was carried out in a water environment (pH = 7) and visible light with quite good results ($t_{1/2} = 2.17$ min); this can expand the application scope of Zr–MOFs in general and UiO-66C/g- C_3N_4 in particular.

Table 3.16. Ability to decompose DMNP using different catalytic materials

Material	Reactive environment	Half-life $t_{1/2}$ (minutes)
UiO-66	NEM (0.45 M, pH =10)	40.00
PP/ZnO/UiO-66–NH ₂	NEM (0.45 M, pH = 10)	4.80
Zr–MOFilter UiO-66–NH ₂	NEM (0.45 M, pH =10)	2.40
UiO-66–NH ₂	NEM (0.45 M, pH =10)	2.80
Graphene/UiO-66–NH ₂	NEM (0.45 M, pH = 10)	1.60
UiO-67	NEM (0.45 M, pH = 10)	4.50
NU-1000	NEM (0.45 M, pH = 10)	3.60
UiO-66C/g- C_3N_4 -30%	Water, pH=7	2.17
4%Ti–MOF-808(Zr)	NEM (0.45 M, pH = 9)	0.25

CONCLUSION AND RECOMMENDATIONS

CONCLUSION

1. The thesis has synthesized TiO_2 nanomaterial and 9 types of Zr-MOFs with 3 different bond types including 12 bond types (UiO-66C, UiO-66C/g- C_3N_4 , UiO-66, UiO-66- NH_2 , UiO-67 and, Zr-NDC), 8 bond types (NU-1000), and 6 bond types (MOF-808(Zr) and Ti-MOF808(Zr)). Among them, UiO-66C and UiO-66C/g- C_3N_4 are synthesized using an H_2BDC linker prepared from recycled PET (polyethylene terephthalate) plastic. Among the synthesized materials, MOF-808(Zr) and, Ti-MOF-808(Zr) have specific surface areas respectively of $1756 \text{ m}^2/\text{g}$ and $1741 \text{ m}^2/\text{g}$ are larger than TiO_2 ($139 \text{ m}^2/\text{g}$) and individual Zr-MOFs ($583 \div 1685 \text{ m}^2/\text{g}$) and are thermally stable above 500°C (Zr), Ti-MOF-808(Zr) ($\sim 100 \text{ nm}$), and UiO-66C, UiO-66C/g- C_3N_4 ($80 \div 120 \text{ nm}$) and are smaller than other synthesized materials.

2. The catalytic activity of nano TiO_2 -100 was determined under conditions with a catalytic content of 30 g/L , in a 0.45 M NEM buffer solution, showing that this material is capable of photocatalytic decomposition to 96.14% after 120 min of reaction. The study also showed that the conversion efficiency of DMNP increased when irradiated with light radiation, increasing from 75.34% (in dark) to 96.14% (in light). This proves that combining hydrolysis and photocatalysis increases the efficiency of DMNP conversion with TiO_2 -100 nanomaterial.

3. Determine the catalytic activity of materials UiO-66C and UiO-66C/g- C_3N_4 under optimal conditions with a catalyst content of 4.20 g/L , water environment ($\text{pH} = 7$), showing the maximum DMNP photocatalytic decomposition efficiency reached 98.9% (60 min) on UiO-66C/g- C_3N_4 -30%, larger than that on UiO-66C (50%) with a half-life of 2.17 min . This result shows that adding UiO-66C to g- C_3N_4 increases the ability to absorb visible light radiation and limits the recombination of electron/hole pairs of the hybrid material, thereby increasing the degradation efficiency of DMNP. Initially propose the mechanism of DMNP decomposition on the catalysts UiO-66C/g-

C₃N₄-30% showed that $\cdot\text{O}^{2-}$, h^+ and $\cdot\text{OH}$ might be the main active site species in the degradation of DMNP.

4. Compare the DMNP photocatalytic decomposition activity of MOF-808(Zr) and 4%Ti–MOF-808(Zr) under appropriate environmental conditions of 0.45 M N-ethylmorpholine buffer solution, pH = 9, and catalyst content of 2.72 g/L. It shows that the half-life of DMNP decreased from 0.47 minutes on MOF-808(Zr) to 0.25 min on 4%Ti–MOF-808(Zr), and the complete decomposition time (100%) of DMNP decreased from 3.00 min for MOF-808(Zr) to 1.34 min for 4%Ti–MOF-808(Zr). The increased catalytic activity of Ti–MOF-808(Zr) is due to the increased amount of Lewis acid center that plays a decisive role in the DMNP decomposition efficiency when there is the presence of Ti^{4+} ions in the Ti–MOF-808 (Zr) material. Initially propose the mechanism of DMNP decomposition on the catalysts 4%Ti–MOF-808(Zr) studies showed that the Lewis acid centers in the 4%Ti–MOF-808(Zr) catalyst can play a decisive role in the decomposition of DMNP.

5. Research on reuse durability shows that 4%Ti–MOF-808(Zr) material maintains DMNP decomposition efficiency of over 98% after 6 reaction cycles. Meanwhile, UiO-66C/g-C₃N₄-30% also retains efficiency above 98% after 5 cycles of use.

RECOMMENDATIONS

This study initially evaluated the ability to decompose the organophosphorus nerve agent simulant DMNP using nano TiO₂, UiO-66C/g-C₃N₄-30%, and 4%Ti–MOF-808(Zr). The results were shows that UiO-66C/g-C₃N₄-30% and 4%Ti–MOF-808(Zr) have the ability to be processed quickly, effectively, and the ability to be reused. To have comprehensive assessments of the ability to treat organophosphorus nerve agents, further research is needed on other simulants of this type of toxin. Besides, it is also necessary to research a number of other organophosphorus compounds to be able to evaluate, perfect, and expand the processing objects of these materials.

NEW CONTRIBUTIONS OF THE THESIS

(1) Successfully synthesizing the UiO-66C/g-C₃N₄-30% photocatalyst using H₂BDC as a linker made from waste polyethylene terephthalate (PET). Successfully integrating UiO-66C with g-C₃N₄ boosted the DMNP conversion efficiency from about 50% with UiO-66C to 98.9% with UiO-66C/g-C₃N₄-30% in an aqueous environment, under visible light irradiation conditions.

(2) The bimetallic catalyst 4%Ti-MOF-808(Zr) was successfully synthesized by doping Ti onto the MOF-808(Zr) framework. This catalyst has a fast processing ability (the half-life of DMNP is 0.25 min) and high efficiency (100% degradation of DMNP in 1.34 min), which is better than the reported metal-organic framework materials.

(3) The factors influencing catalytic activity were systematically investigated, leading to the identification of suitable conditions for the rapid and effective degradation of DMNP using two types of catalysts: UiO-66C/g-C₃N₄-30% and 4%Ti-MOF-808(Zr). Additionally, an initial proposal for the degradation mechanism of DMNP on the UiO-66C/g-C₃N₄-30% and 4%Ti-MOF-808(Zr) catalysts was suggested. The photocatalytic mechanism of UiO-66C/g-C₃N₄-30% implies that $\cdot\text{O}^{2-}$, h^+ , and $\cdot\text{OH}$ may serve as the main active species. Meanwhile, the Lewis acid sites in the 4%Ti-MOF-808(Zr) catalyst could play a crucial role in the degradation of DMNP. This is an important step, providing the scientific basis for the effective synthesis of materials for the creation of chemical agents that detoxify organophosphorus nerve agents in the military field and expanding the application of organophosphorus compound treatment in industrial and civilian uses.